**Smart Structures and Systems**, *Vol. 15, No. 2 (2015) 375-393*
DOI: http://dx.doi.org/10.12989/sss.2015.15.2.375 

# Local dynamic characteristics of PZT impedance interface on tendon anchorage under prestress force variation

Thanh-Canh Huynh[a], Kwang-Suk Lee[b] and Jeong-Tae Kim[*]

*Department of Ocean Engineering, Pukyong National University, 599-1 Daeyeon 3-dong, Nam-gu, Busan 608-737, Republic of Korea*

*(Received November 30, 2014, Revised January 13, 2015, Accepted January 16, 2015)*

**Abstract.** In this study, local dynamic characteristics of mountable PZT interfaces are numerically analyzed to verify their feasibility on impedance monitoring of the prestress-loss in tendon anchorage subsystems. Firstly, a prestressed tendon-anchorage system with mountable PZT interfaces is described. Two types of mountable interfaces which are different in geometric and boundary conditions are designed for impedance monitoring in the tendon-anchorage subsystems. Secondly, laboratory experiments are performed to evaluate the impedance monitoring via the two mountable PZT interfaces placed on the tendon-anchorage under the variation of prestress forces. Impedance features such as frequency-shifts and root-mean-square-deviations are quantified for the two PZT interfaces. Finally, local dynamic characteristics of the two PZT interfaces are numerically analyzed to verify their performances on impedance monitoring at the tendon-anchorage system. For the two PZT interfaces, the relationships between structural parameters and local vibration responses are examined by modal sensitivity analyses.

**Keywords:** local dynamic; PZT interface; tendon anchorage; prestress force; impedance signature; modal analysis; modal sensitivity

## 1. Introduction

Damage detection in structural systems via monitoring impedance signatures has been studied by many researchers (Liang *et al.* 1994, Park *et al.* 2001, Zagral and Giurgiutiu 2001, Bhalla and Soh 2003, Yang and Lu 2008, Kim *et al.* 2006, Providakis *et al.* 2014, Li *et al.* 2014). The 'so-called' impedance-based method utilizes the electro-mechanical (EM) impedance of a coupled PZT (Lead Zirconate Titanate)-structure system to identify the change in dynamic characteristics at the local structural region. Relative to low-frequency vibration responses, the EM impedance response of a high frequency range has been promising to monitor small incipient damage at the local critical members.

Recently, the impedance-based method has been applied for monitoring the prestress-loss in tendon-anchorage connections (Kim *et al.* 2009, Kim *et al.* 2010, Nguyen and Kim 2012, Huynh and Kim 2014). A limitation of their studies was on setting the frequency band sensitive to the

∗Corresponding author, Professor, E-mail: idis@pknu.ac.kr
[a] Ph.D. Student, E-mail: ce.huynh@gmail.com
[b] MS. Student, E-mail: icsa88@gmail.com


http://www.techno-press.org/?journal=sss&subpage=8 ISSN: 1738-1584 (Print), 1738-1991 (Online)

variation of the prestress forces. The effective frequency band was even over 800 kHz for a mono-tendon anchorage under compressive forcing about 100 kN (Kim *et al.* 2010). To overcome the disadvantage, Nguyen and Kim (2012) developed an impedance-sensitive PZT interface technique which could reduce the frequency band to below 100 kHz and also the need of a high performance impedance analyzer. However, this design of PZT interface should be installed during the construction of the anchorage subsystem, so it is impossible to apply it into existing joint members.

In order to overcome the above-mentioned drawbacks, Huynh and Kim (2014) proposed a portable PZT interface that could be mounted on (and detached from) the surface of bearing plates. The proposed PZT-interface technique was experimentally evaluated for a lab-scaled cable structure to monitor the change in impedance responses caused by the change in prestress forces. Also, a numerical impedance analysis was conducted to examine the performance of a new interface device (Huynh *et al.* 2014). Despite those research attempts, however, there still exists a need to verify the feasibility of monitoring impedance responses via the portable PZT interface mounted on the bearing plate that is subjected to the variation of the anchoring forces. In other words, the relationship between the anchor force and the structural response of the PZT interface should be proved in order to justify the mountable PZT interface-based impedance monitoring of the prestress-loss.

In this study, local dynamic characteristics of the mountable PZT interfaces are numerically analyzed to verify their feasibility on impedance monitoring of the prestress-loss in the tendon anchorage subsystems. The following approaches are implemented to achieve the objective. Firstly, a prestressed tendon-anchorage system with mountable PZT interfaces is described. Two types of mountable interfaces which are different in geometric and boundary conditions are designed for impedance monitoring in the tendon-anchorage subsystems. Secondly, laboratory experiments are performed to evaluate the impedance monitoring via the two mountable PZT interfaces placed on the tendon-anchorage under the variation of prestress forces. Impedance features such as frequency-shifts and root-mean-square-deviations are quantified for the two PZT interfaces. Finally, local dynamic characteristics of the two PZT interfaces are numerically analyzed to verify their performances on impedance monitoring at the tendon-anchorage subsystem. For the two PZT interfaces, the relationships between structural parameters and local vibration responses are examined by modal sensitivity analyses. Peak impedance responses and their corresponding structural parameters sensitive to the variation of prestress forces in the anchorage subsystem are identified by analyzing local dynamic characteristics and experimentally measured impedance responses.

## 2. Tendon-anchorage system with mountable interfaces

### *2.1 Two types of mountable interfaces*

The mountable PZT interface is designed to monitor EM impedance signatures of the prestressed tendon-anchorage system. As shown in Fig.1, the PZT interface is mounted on the bearing plate that is subjected to the variation of the anchoring forces. For tendon-anchorage systems, the effect of the bearing plate on the interface's local resonance is assumed to be negligibly small. This assumption comes from the fact that the PZT interface has much smaller flexural stiffness than the bearing plate. In this study, the PZT interface is designed to deal with

1V-amplitude excitation and impedance monitoring using wireless sensor technology which offers an automated and cost-efficient monitoring systems (Lynch *et al.* 2006, Rice *et al.* 2010, Kim *et al.* 2014), and allows the frequency range of 10-100 kHz (Mascarenas *et al.* 2007). The PZT interface's structural properties are basically selected to fulfill the limitation of the wireless impedance monitoring.

For experimental verification, two types of PZT interfaces were designed to examine their performances for impedance monitoring. Fig. 2 shows the two interfaces and their geometries. The aluminum interfaces have the fixed-fixed boundary condition by two outside contact bodies and the flexible beam section in the middle, as shown in the side view. The fixed boundary conditions are simulated by contact surfaces bonded on the bearing plate. The fixed sections of the two interfaces have the following dimensions: 35×18×6 $mm^3$ (Interface 1) and 35×33×6 $mm^3$ (Interface 2). The unbonded beam sections, where the PZTs are installed, are designed to allow flexural vibration responses and piezoelectric deformation in longitudinal and lateral directions. The unbonded sections have the following dimensions: 30×18×5 $mm^3$ (Interface 1) and 30×33×5 $mm^3$ (Interface 2). It is noted that the bonding area of Interface 2 is larger (about 1.8 times) than that of Interface 1. As shown in Fig. 3, the PZT interfaces are installed at the right end of the bearing plate of the tendon-anchorage system. A mono-tendon of $\phi$15.2 mm is anchored by an anchor head of $\phi$45 mm on the bearing plate of 100×100×10 $mm^3$. The material properties of the tendon-anchorage and the PZT interfaces are listed in Table 1. Also, the EM properties of PZT-5A patch used for the experiment are listed in Table 2.

To verify the feasibility of monitoring impedance responses via the interface, at least two relationships should be examined for the 'PZT interface-bearing plate-anchor force' model. Firstly, the change of the tendon-anchorage force may cause the change of the anchorage subsystem's equivalent structural properties which result in the change in dynamic characteristics such as local impedance responses. So it is needed to prove that the bearing plate's structural properties such as geometrical and traction boundary conditions are changed due to the prestress-loss. Secondly, the change of the bearing plate's structural properties may cause the change of structural properties (i.e., geometrical and stress boundary conditions) of the PZT interface that is fixed on the surface boundary of the bearing plate. Consequently, this will prove that local dynamic responses of the PZT interface are changed due to the change of the anchor force.

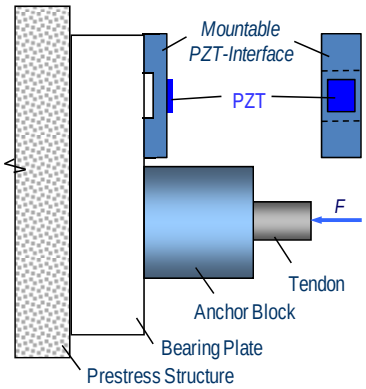


Fig. 1 Prestressed tendon-anchorage system with a mountable PZT-interface (Huynh and Kim 2014)

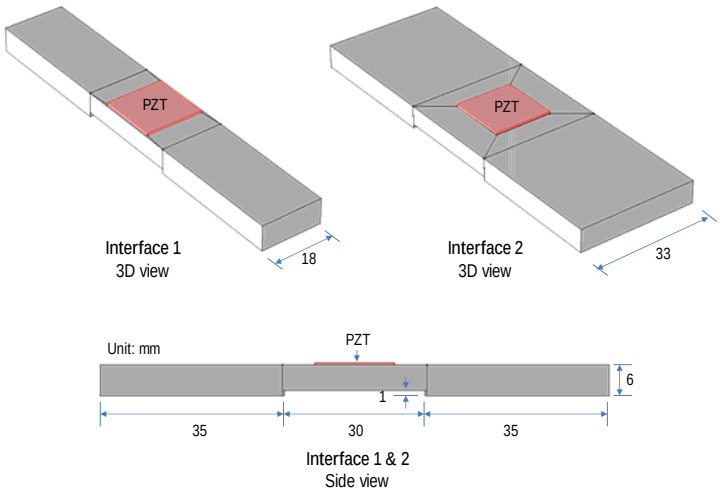


Fig. 2 Two mountable PZT interfaces and their geometries

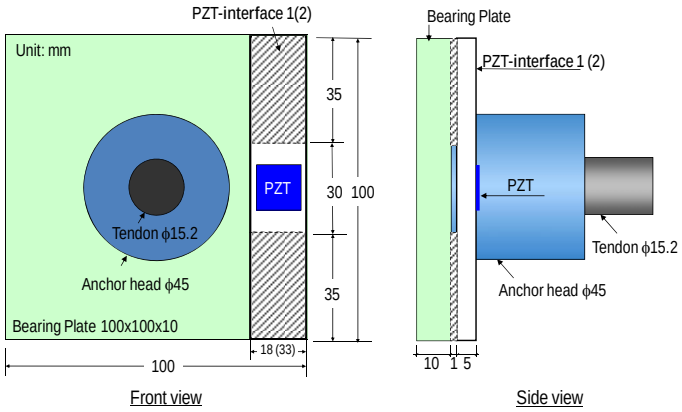


Fig. 3 Geometry of tendon-anchorage equipped with mountable PZT interfaces (Huynh and Kim 2014)

Table 1 Material properties of PZT interface, bearing plate and anchor head

| Parameters | PZT-Interfaces 1 & 2 | Bearing plate and anchor head |
|---|---|---|
| Young's modulus, $E$ (GPa) | 70 | 200 |
| Poisson's ratio, $\upsilon$ | 0.33 | 0.3 |
| Mass density, $\rho$ (kg/m$^3$) | 2700 | 7850 |
| Damping loss factor, $\eta$ | 0.02 | 0.02 |

Table 2 Material properties of PZT patch (Efunda, Inc. 2010)

| Parameters | Value |
|---|---|
| Elastic compliance, $S_{ijkl}^{E}$ ($m^2$/N) | $\begin{pmatrix} 16.4 & -5.74 & -7.22 & 0 & 0 & 0 \\ -5.74 & 16.4 & -7.22 & 0 & 0 & 0 \\ -7.22 & -7.22 & 18.8 & 0 & 0 & 0 \\ 0 & 0 & 0 & 47.5 & 0 & 0 \\ 0 & 0 & 0 & 0 & 47.5 & 0 \\ 0 & 0 & 0 & 0 & 0 & 44.3 \end{pmatrix} \times 10^{-12}$ |
| Dielectric coupling constant, $d_{kij}$ (C/N) | $\begin{pmatrix} 0 & 0 & -171 \\ 0 & 0 & -171 \\ 0 & 0 & 374 \\ 0 & 584 & 0 \\ 584 & 0 & 0 \\ 0 & 0 & 0 \end{pmatrix} \times 10^{-12}$ |
| Permittivity, $\varepsilon_{jk}^{T}$ (Farad/m) | $\begin{pmatrix} 1730 & 0 & 0 \\ 0 & 1730 & 0 \\ 0 & 0 & 1700 \end{pmatrix} \times \left(8.854 \times 10^{-12}\right)$ |
| Mass density, $\rho$ (kg/$m^3$) | 7750 |
| Damping loss factor, $\eta$ | 0.005 |
| Dielectric loss factor, $\delta$ | 0.015 |

### *2.2 Impedance measurement via two interfaces*

Laboratory experiments were carried out for a tendon-anchorage system with the two mountable PZT-interfaces (i.e., Interfaces 1 and 2) as shown in Fig. 4. A tendon cable of 6.4 m was anchored by bearing plates at both ends. Tension force was introduced into the cable by a stressing jack as the cable was anchored at one end and pulled out at the other. A load cell was installed at one tendon-anchorage to measure the actual cable force. For each test, the PZT patch on the interface was excited by a harmonic excitation voltage with 1V-amplitude, and the impedance signature was measured by an impedance analyzer HIOKI 3532. The tendon cable was first pre-tensioned to T1 = 49.05 kN and reduced into T2 = 39.2 kN, T3 = 29.4 kN and T4 = 19.6 kN for prestress-loss simulation.

Impedance responses of the two PZT interfaces were measured in the frequency range 10-100 kHz. The frequency range was examined to evaluate the feasibility of the two PZT interfaces on impedance monitoring using wireless technology which allows only the frequency range of 10-100 kHz (Mascarenas *et al.* 2007). In general, the real part of EM impedance contains much more information about structural behaviors than imaginary part (Sun *et al.* 1995, Park *et al.* 2003). Hence, real part of impedance response is examined for tendon force-loss monitoring. In practice, the electric current $I(\omega)$ is measured and then it is utilized to calculate the EM impedance as follows (Liang *et al.* 1994 and 1996)

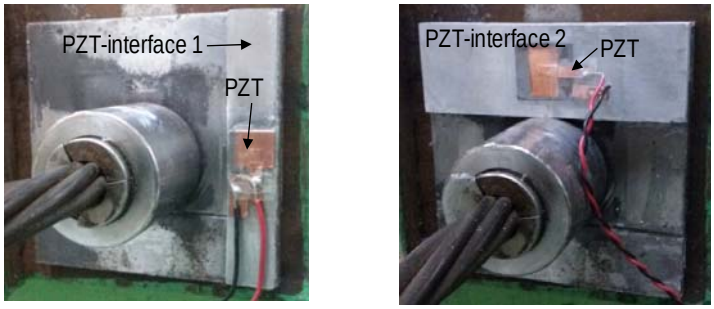


Fig. 4 Tendon-anchorage connection with two PZT interfaces

$$Z(\omega)=\frac{V}{I}=\left\{i\omega\frac{w_a l_a}{t_a}\left[\hat{\varepsilon}_{33}^{T}-\frac{1}{Z_a(\omega)/Z_s(\omega)+1}d_{3x}^{2}\hat{Y}_{xx}^{E}\right]\right\}^{-1} \quad (1)$$

where $\hat{Y}_{xx}^{E}=(1+i\eta)Y_{xx}^{E}$ is the complex Young's modulus of the PZT patch at zero electric field; $\hat{\varepsilon}_{xx}^{T}=(1-i\delta)\varepsilon_{xx}^{T}$ is the complex dielectric constant at zero stress; $d_{3x}$ is the piezoelectric coupling constant at zero stress; and $w_a$, $l_a$, and $t_a$ are the width, length, and thickness of the piezoelectric transducer, respectively. The EM impedance, $Z(\omega)$, is a combining function of the structural mechanical (SM) impedance of the host structure, $Z_s(\omega)$, and the electrical impedance of the piezoelectric patch, $Z_a(\omega)$. Therefore, the change in structural parameters ($k$, $m$, $c$) can be represented by the change in EM impedance.

## 3. Impedance monitoring performance of two interfaces

### *3.1 Impedance responses of two interfaces*

#### *3.1.1 Impedance response of interface 1*

The performance of impedance monitoring via the mountable PZT interface was examined for the prestress forces (T1 – T4). Fig. 5 shows real impedance signatures of Interface 1 in the wide frequency range 10-100 kHz (901 interval points) for the reference state T1 (49.05 kN) and three other cases T2-T4. Also, two resonant frequency bands of 18-21 kHz (501 interval points) and 81-84 kHz (501 interval points) corresponding to the two peaks are taken into account. It is observed that both Peak 1 and Peak 2 are varied as tendon forces decrease. This implies that the contribution of the SM impedance to the EM impedance is considerable in the two resonant frequency ranges, as explained in Eq. (1).

The resonant frequencies tend to shift left, according to the decrement of the tendon force. This indicates that the modal stiffness of Interface 1 is decreased with the reduction of the tendon force. As the tendon force is reduced about 60% from T1 to T4, the peak frequency shifts very small, not greater than 0.5% for the first resonant frequency ($f_1$) and 0.2% for the second one ($f_2$), as shown in Fig. 7(a). However, the change in resonant frequencies could not be distinguished in some cases.

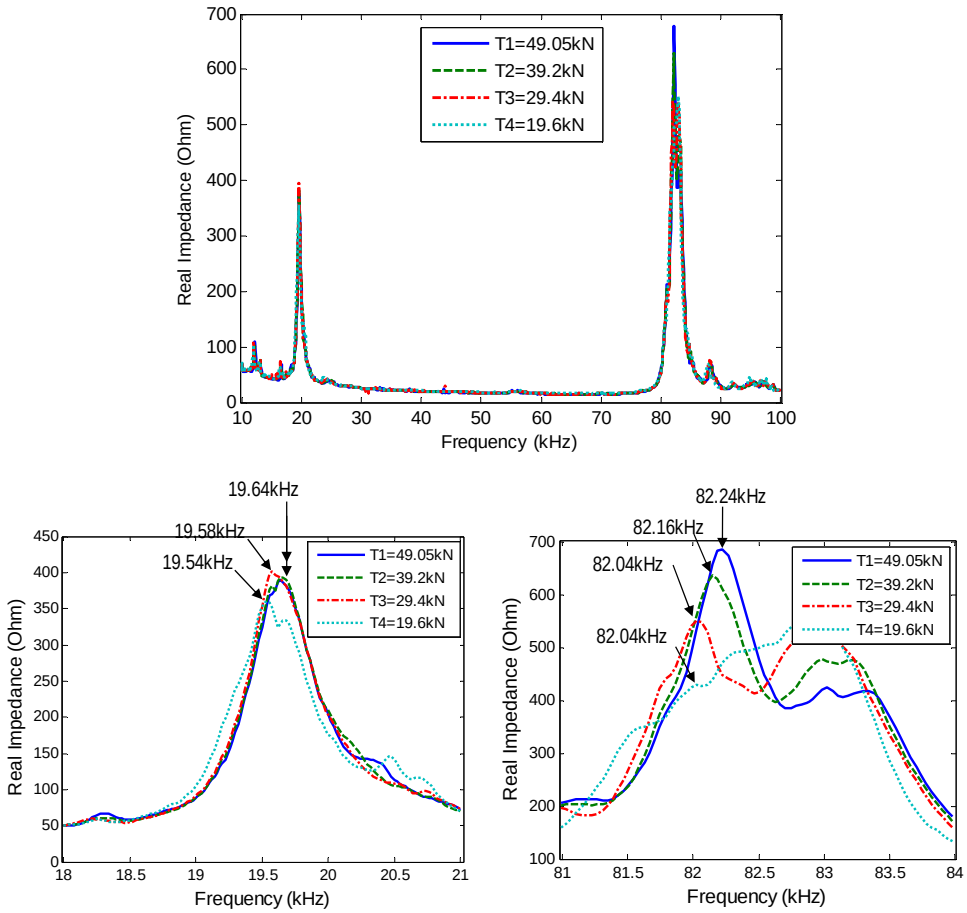


Fig. 5 Impedance responses measured from Interface 1 under various forces

### *3.1.2 Impedance Response of Interface 2*

Fig. 6 shows real impedance signatures of Interface 2 in the frequency range 10-100 kHz (901 interval points) for the four cases T1-T4. Also, two resonant frequency bands of 14-20 kHz (501 interval points) and 34-40 kHz (501 interval points) corresponding to the two peaks are considered. It is observed that both Peak 1 and Peak 2 are sensitively varied when the prestress force decreases. This implies the contribution of the SM to the EM impedance is considerable in the two resonant frequency ranges, as explained in Eq. (1).

The resonant frequencies tend to shift left according to the decrement of prestress force. This indicates that the modal stiffness of Interface 2 is decreased with the reduction of the tendon force. When the tendon force is reduced to 60% (from T1 to T4), the frequency shifts relatively high as 2.8% for the first resonant frequency ($f_1$) and 3.2% for the second one ($f_2$), as shown in Fig. 7(b). As the tendon forces were changed, Interface 2 revealed much higher sensitivity in the frequency-shift as compared to Interface 1.

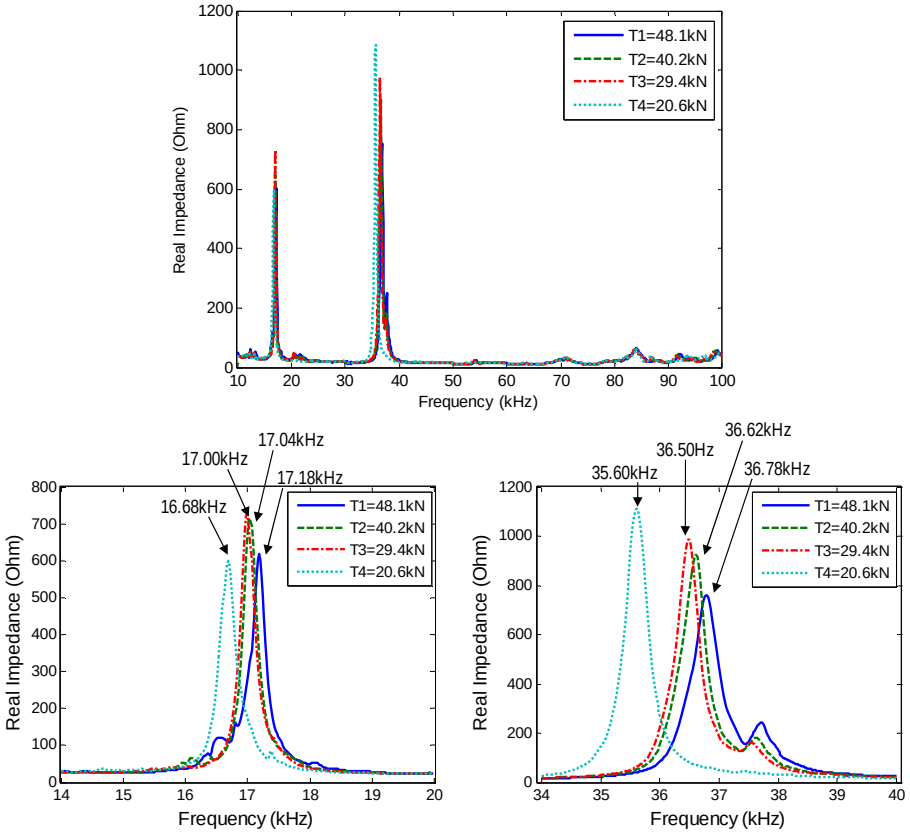


Fig. 6 Impedance responses measured from Interface 2 under various forces

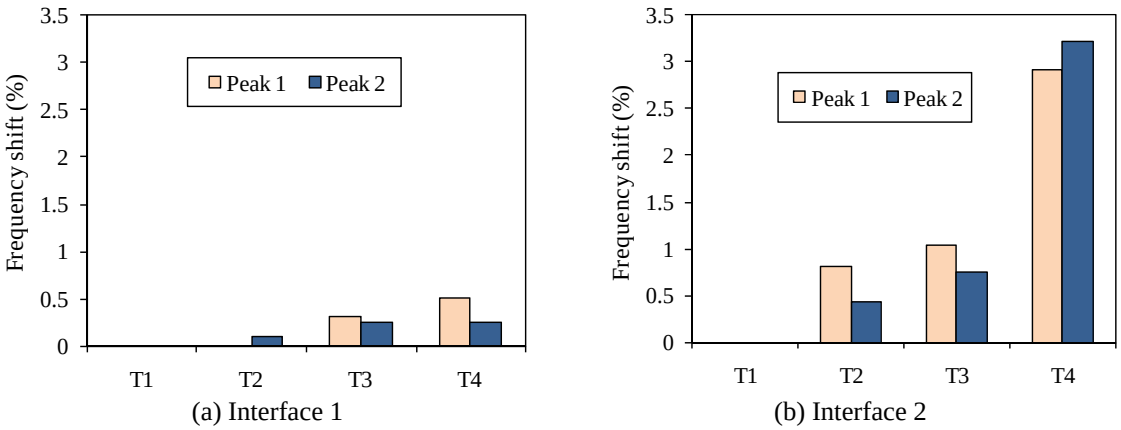


Fig. 7 Frequency shifts measured from Interfaces 1 and 2 under various forces

### *3.2 RMSD quantification of two interfaces*

To quantify the change in EM impedance, the root mean square deviation (RMSD) index is utilized (Sun *et al*. 1995). RMSD index is calculated as

$$RMSD\left(Z,Z^*\right)=\sqrt{\sum_{i=1}^{N}\left[Z^*\left(\omega_i\right)-Z\left(\omega_i\right)\right]^2\Big/\sum_{i=1}^{N}\left[Z\left(\omega_i\right)\right]^2} \tag{2}$$

where $Z(\omega_i)$ and $Z^*(\omega_i)$ are the impedances measured before and after a structural change for the $i^{th}$ frequency, respectively; and N denotes the number of frequency points in the sweep.

Basically, the RMSD is equal to 0 if intact, and larger than 0 if the structural change occurs. However, due to experimental errors, the RMSD may be larger than 0 although the structural change is not occurred. To deal with the uncertain conditions, the control chart analysis is used for decision-making out of RMSD values. The upper control limit ($UCL_{RMSD}$) is adopted for alerting the structural change, as follows

$$UCL_{RMSD}=\mu_{RMSD}+3\sigma_{RMSD} \tag{3}$$

where $\mu_{RMSD}$ and $\sigma_{RMSD}$ are mean and standard deviation of RMSD data set at the reference condition, respectively. The calculation of RMSD is outlined in three steps: firstly, n impedance signals are measured at a structural change condition; secondly, RMSD values for n impedance signals are computed by Eq. (2), then a set of RMSD values is obtained; and finally, $UCL_{RMSD}$ of the RMSD value is calculated using Eq. (3). The structural change is indicated when the RMSD values are larger than the $UCL_{RMSD}$. Otherwise, there is no indication.

#### *3.2.1 RMSD Index of Interface 1*

Generally, RMSD is sensitive to both horizontal shift and vertical shift of impedance signature. As observed in Fig. 5, the change in tendon forces causes not only vertical shift but also horizontal shift of impedance responses as measured by Interface 1. Therefore, RMSD indices are examined for four tension levels. Fig. 8 shows RMSD indices calculated according to the increment of tendon force-loss for the two narrow frequency ranges (i.e., 18-21 kHz and 81-84 kHz) corresponding to the two peak impedance responses. The RMSD indices increase gradually as the tendon forces are reduced from T1 to T4. The RMSD indices of the second peak's frequency range (i.e., 81-84 kHz) show a little more sensitive indication of tension-loss than that of the first peak's frequency range (18-21 kHz).

#### *3.2.2 RMSD Index of Interface 2*

As observed in Fig. 6, the change of tendon forces results in sensitive shifts of impedance responses as measured by Interface 2. Fig. 9 shows RMSD indices calculated according to the increment of tension-loss for the two narrow frequency ranges (i.e., 14-20 kHz and 34-40 kHz) corresponding to the two peak impedance responses. The RMSD indices increase proportionally as the tendon forces are reduced from T1 to T4. The RMSD indices of the first peak's frequency range (i.e., 14-20 kHz) and those of the second peak's frequency range (i.e., 34-40 kHz) show both very sensitive indications of the tension-loss. The RMSD indices of Interface 2 indicate the structural changes about 5-10 times more sensitively as compared to those of Interface 1. This result indicates that Interface 2 can better detect the change in impedance responses due to the loss of tension forces.

## 4. Dynamic characteristics of mountable PZT interfaces

### 4.1 Impedance responses of two interfaces

As shown in Fig. 10, the SM impedance response can be explained from the interaction between the PZT patch and the structure (e.g., the interface body). The SM impedance of the structure is defined as the ratio of force $F(\omega)$ to velocity $\dot{u}(\omega)$ as follows (Liang *et al*. 1994)

$$Z_s(\omega) = \frac{F(\omega)}{\dot{u}(\omega)} = c + m\frac{\omega^2 - \omega_n^2}{\omega} i \tag{4}$$

where $c$ and $m$ are the damping coefficient and the mass of the interfacing structure with the PZT patch, respectively; $\omega_n$ is the angular natural frequency of the interface structure; and $\omega$ is the angular frequency of the excitation voltage.

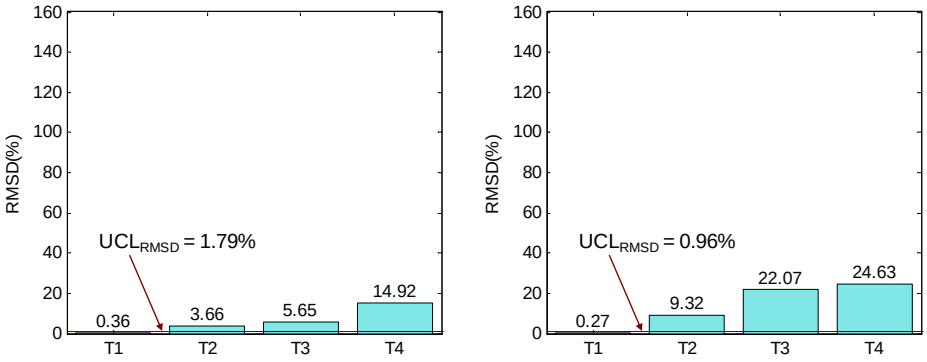


(a) Frequency range 18-21 kHz (Peak 1) (b) Frequency range 81-84 kHz (Peak 2)

Fig. 8 RMSD index of Interfaces 1 under various forces

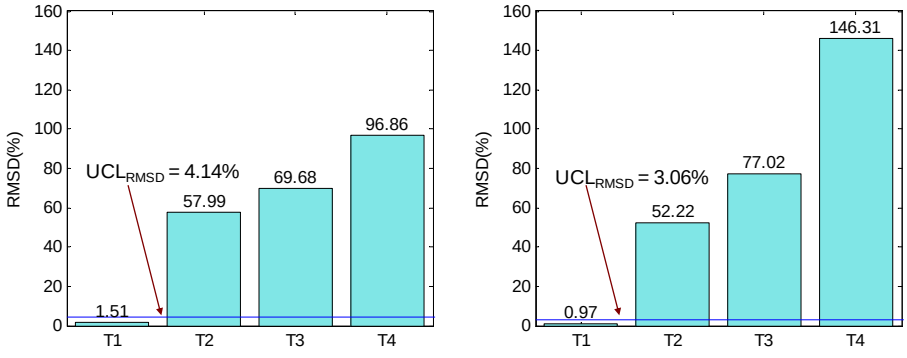


(a) Frequency range 14-20 kHz (Peak 1) (b) Frequency range 34-40 kHz (Peak 2)

Fig. 9 RMSD index of Interfaces 2 under various forces

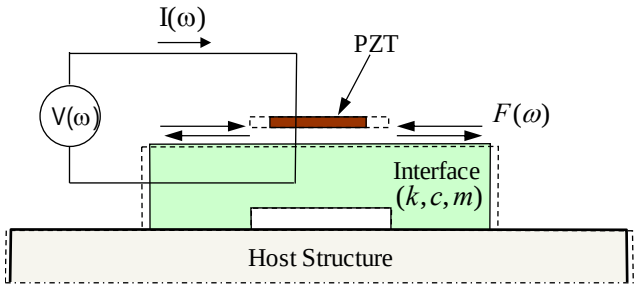


Fig. 10 PZT interface-structure model for SM impedance response

As shown in Eq. (4), the SM impedance is a function of structural properties (i.e., mass, damping, and stiffness), so that the change in structural parameters can be inversely interpreted by the change in the SM impedance. As shown in Fig. 10, an input harmonic voltage *V(ω)* induces a deformation of the PZT due to the inverse piezoelectric effect. Then a force *F(ω)* against that deformation is induced into the structure (i.e., the interface bodies) and the PZT as well, because the PZT is surface-bonded to the interface structure. On the analogous manner, the force *F(ω)* is changed when the PZT is statically pre-deformed due to the change in the geometrical interface's properties which may be caused by the change in the host structure's geometrical properties (as illustrated in Fig. 10).

### *4.2 Local dynamic responses of two interfaces*

Dynamic characteristics of the two PZT interfaces are examined to understand the relationship between structural properties of the interfaces and their sensitive resonant frequencies of impedance signatures. Note from Figs. 5 and 6 that the impedance signatures in the non-resonant regions 21-81 kHz (for Interface 1) and 20-34 kHz (for Interface 2) are almost unchanged due to the change of tendon forces. This means that the contribution of the SM impedance to the EM impedance (see Eq. (1)) is negligibly small as compared to the two peak resonant-frequency responses. Note from Eq. (1) that the impedance signatures in those frequency ranges are associated with the SM impedance responses of the PZT interfaces and the tendon-anchorage system. Therefore, it is needed to prove that the two peak frequencies are related to the PZT interfaces' structural properties (e.g., material, geometrical and boundary conditions). It is also needed to prove that the two peak frequencies are changed due to the change of the tendon forces.

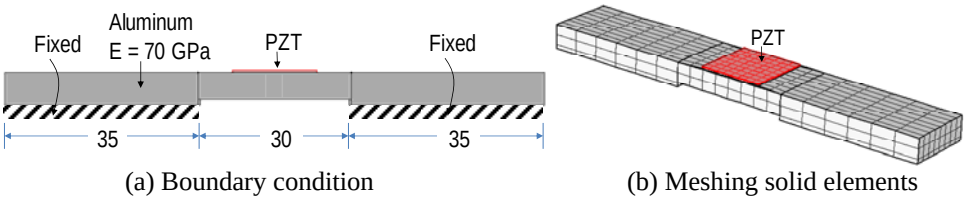


(a) Boundary condition (b) Meshing solid elements

Fig. 11 FE model of mountable PZT interface

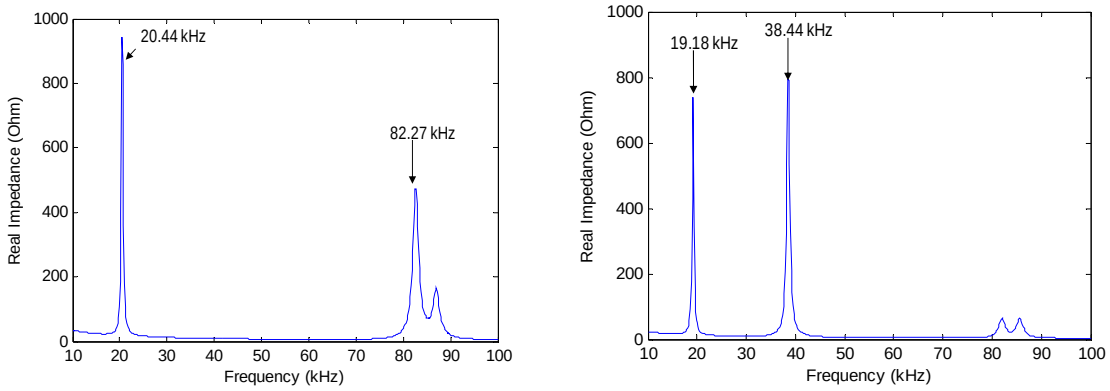


(a) Interface 1 (b) Interface 2

Fig. 12 Numerical impedance responses of two PZT interfaces

A finite element (FE) model of the PZT interface is established by the commercial package, COMSOL Multiphysics (2013). Research attempts have been made to simulate the numerical EM impedance by using COMSOL (Kim *et al.* 2012, Ho *et al.* 2014). Fig. 11(a) shows the geometry and the fixed-fixed boundary condition of the PZT interface. The selection of the fixed boundary condition was based on the fact that the flexural stiffness of the PZT interface is much smaller than that of the bearing plate, as stated previously. In FE modeling, the interface was discretized by 3D elastic solid elements, as shown in Fig. 11(b). The meshing includes 608 solid elements: 64 elements for the PZT patch and 544 elements for the interface body. The properties of the aluminum interface (listed in Table 1) are specified for the FE model. Also, the PZT patch is added by the piezoelectric material, PZT-5A (listed in Table 2). To acquire the EM impedance responses, a harmonic excitation voltage with an amplitude of 1 V was simulated to the top surface of the PZT patch element, and the bottom one was set as the ground electrode.

Impedance responses of the two PZT interfaces were numerically analyzed, as shown in Fig. 12. The numerical impedance responses of the two interfaces were consistent as compared to the experimental impedance responses (shown in Figs. 5 and 6). Interface 1 shows the first and second peak frequencies at 20.44 kHz and 82.27 kHz, respectively. Interface 2 shows the first and second peaks of impedance responses at 19.18 kHz and 38.44 kHz, respectively. The first peaks of the two interfaces are very close in their frequencies; meanwhile, the second peaks of them are quite different from each other. It is noted that the second peak is reduced from 82.27 kHz to 38.44 kHz as the width of the interface is increased from 18 mm to 33 mm, as shown in Fig. 2.

#### *4.2.1 Modal analysis of interface 1*

Numerical modal analyses were performed for Interface 1. The first eight mode shapes representing the local vibration responses of Interface 1 were obtained as shown in Fig. 13. Among them, modes 1, 4 and 5 are out-of-plane longitudinal flexural motions. Modes 2, 6, and 7 are out-of-plane longitudinal twist motions. Mode 3 is an in-plane lateral bending motion. Mode 8 is an out-of-plane lateral flexural motion.

Matching to the piezoelectric deformations of the PZT patch on the interface (as illustrated in Fig. 10), the first longitudinal flexural motion (mode 1) is identical to the first impedance peak that

represents the first resonant frequency. Also, the first lateral flexural motion (mode 8) is identical to the second impedance peak that represents the second resonant frequency. From the comparison between Figs. 12 and Fig. 13, two modal shapes of Interface 1 corresponding to the two resonant impedance peaks were numerically analyzed as 20.366 kHz (mode 1) and 81.527 kHz (mode 8), respectively. It is observed that the first and second peaks of the impedance responses are identical to the modes (i.e., modes 1 and 8) that represent the local vibration responses of the Interface 1.

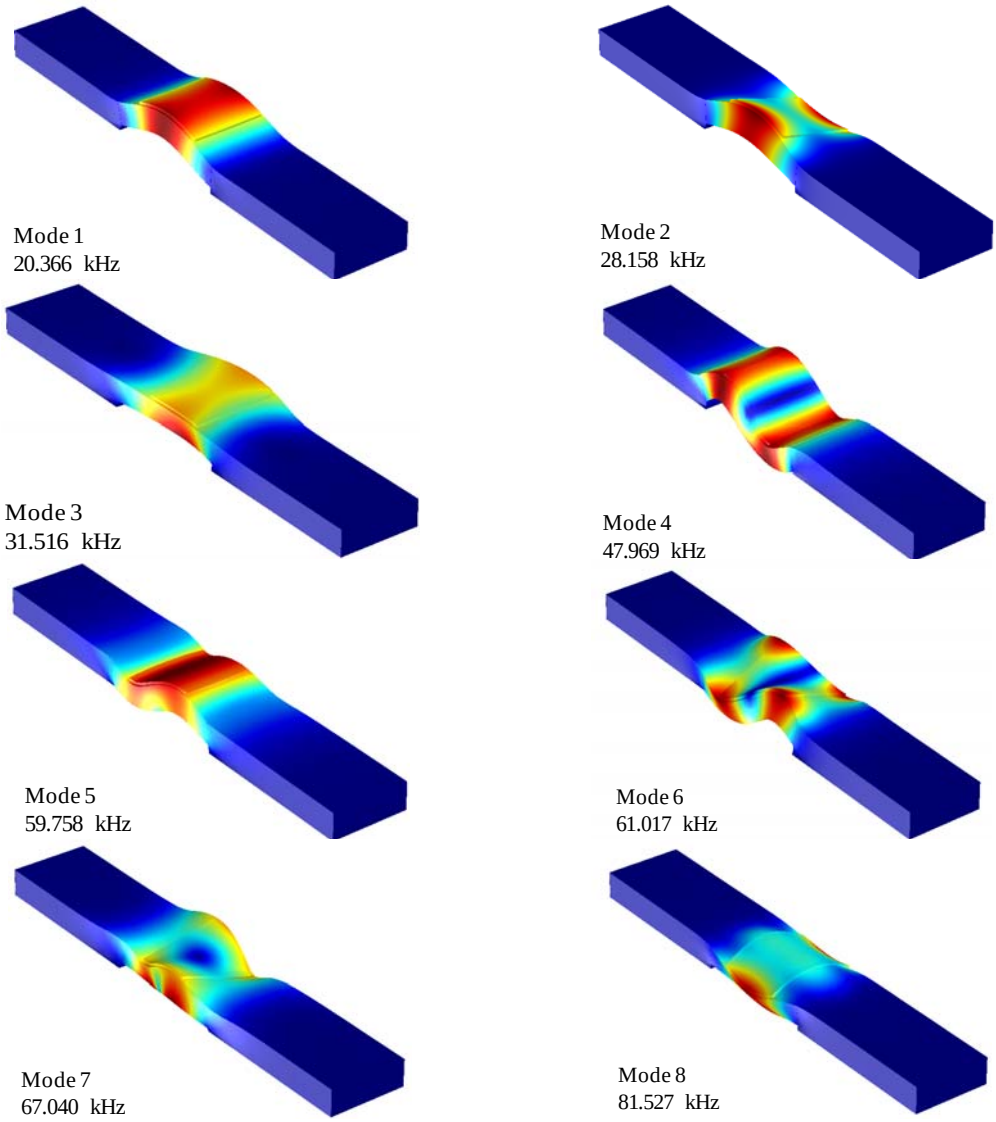


Fig. 13 Interface 1's eight modal shapes corresponding to resonant impedance frequencies

#### 4.2.2 Modal analysis of interface 2

Next, numerical modal analyses were also performed for Interface 2. The first four mode shapes representing the local vibration responses of Interface 2 were obtained as shown in Fig. 14. Among them, mode 1 is an out-of-plane longitudinal flexural motion. Mode 2 is an out-of-plane longitudinal twist motion. Mode 3 is an in-plane lateral bending motion. Mode 4 is out-of-plane lateral flexural motion.

Matching to the piezoelectric deformations of the PZT patch on the interface (as illustrated in Fig. 10), the first longitudinal flexural motion (mode 1) is identical to the first impedance peak that represents the first resonant frequency. Also, the first lateral flexural motion (mode 4) is identical to the second impedance peak that represents the second resonant frequency. From the comparison, two modal shapes of Interface 2 corresponding to the two resonant impedance peaks were numerically analyzed as 19.016 kHz (mode 1) and 37.923 kHz (mode 4), respectively. It is observed that the first and second peaks of the impedance responses are identical to the modes (i.e., modes 1 and 4) that represent the local vibration responses of Interface 2. It is also observed from the two interfaces that the second modal frequencies matching to the second impedance peaks are reduced from 81.527 kHz to 37.923 kHz as the interface's widths are increased from 18 mm (Interface 1) to 33 mm (Interface 2) as shown in Fig. 2.

### 4.3. Modal sensitivity analyses of two interfaces

#### 4.3.1 Modal sensitivity theory

Modal sensitivities of the two PZT interfaces are estimated by using an eigenvalue sensitivity concept proposed by Kim and Stubbs (1995). Suppose $p^*_j$ is an unknown parameter of the $j^{th}$ member of a structure for which $M$ eigenvalues ($\omega^2_{i,m}$, $i = 1,...,M$) are known. Also, suppose $p_j$ is a known parameter of the $j^{th}$ member of a FE model for which the corresponding set of $M$ eigenvalues ($\omega^2_{i,a}$, $i = 1,...,M$) are known. Then the modal sensitivity, $S_{ij}$, of the $i^{th}$ eigenvalue $\omega^2_{i,a}$ with respect to the $j^{th}$ structural parameter $p_j$ is defined as follows

$$S_{ij} = \frac{\delta\omega^2_{i,a}}{\delta p_j}\frac{p_j}{\omega^2_{i,a}} \tag{5}$$

where $\delta p_j$ is the first order perturbation of $p_j$ which produces the variation in eigenvalue $\delta\omega^2_{i,a}$ Once the modal sensitivity is determined, an unknown parameter $p^*_j$ of the $j^{th}$ member of a structure can be determined as follows

$$p^*_j = p_j\left(1+\alpha_j\right) \tag{6}$$

in which $\alpha_j = (\delta p_j/p_j)$ is the fractional change of the structural parameter, and $\alpha_j \geq -1$.

As shown in Fig. 15, the FE model consisted of two member types by regrouping the 544 solid elements of the interface body (as shown in Fig. 11): member 1 (the two outside contact bodies) and member 2 (the inside flexural beam). The structural parameters of the two members are noted as $p_1$ and $p_2$, respectively. Initial values for the geometric properties of the FE model were estimated as the same values as those used for the modal analyses of the PZT interfaces.

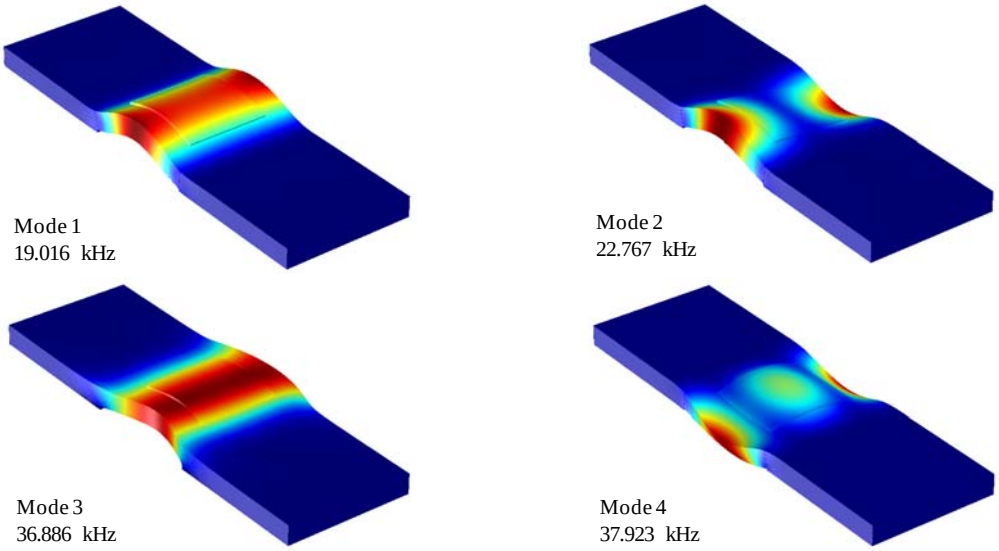


Fig. 14 Interface 2's four modal shapes corresponding to resonant impedance frequencies

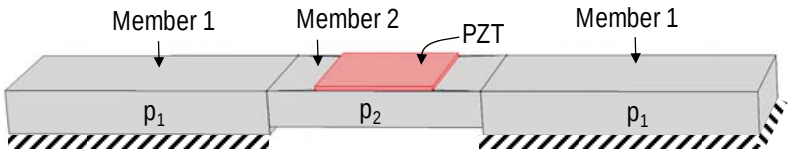


Fig. 15 Member ID of PZT interface

The fractional structural parameter change of the two members may be obtained using the following equation

$$[S]\{\alpha\} = \{Z\} \tag{7}$$

in which $\{\alpha\}$ is a $2\times1$ matrix containing the fractional changes in structural parameters between the undamaged FE model and its corresponding damaged state: $\alpha_1 = \delta p_1 / p_1$ and $\alpha_2 = \delta p_2 / p_2$. Next, $\{Z\}$ is a $2\times1$ matrix containing the fractional changes in two eigenvalues between two systems: $Z_1 = \delta\omega_{1,a}^2 / \omega_{1,a}^2$ and $Z_2 = \delta\omega_{2,a}^2 / \omega_{2,a}^2$. Finally, $[S]$ is a $2\times2$ modal sensitivity matrix.

The sensitivity matrix $[S]$ is numerically determined as follows: (1) Introduce a known severity of damage $\alpha_k$ at the $k^{\text{th}}$ member of the FE model and compute two damaged eigenvalues; (2) compute the fractional changes of eigenvalues, $\{Z\}$, between the undamaged and the FE

model damaged at the $k^{th}$ member; (3) compute the components of the $k^{th}$ column of the $[S]$ matrix by dividing $\{Z\}$ by $\alpha_k$; and (4) generate the $2\times 2$ $[S]$ matrix by repeating steps 1-3 with new damage scenarios up to two members.

#### 4.3.2 Modal sensitivity of interface 1

A FE model was designed for the geometry and boundary conditions of Interface 1. The modal sensitivity matrix was estimated as follows: firstly, two damage scenarios were introduced into the FE model; secondly, two eigenvalues of mode 1 and mode 8 (shown in Fig. 13) were calculated as listed in Table 3; thirdly, the fractional changes of the two eigenvalues were computed and modal sensitivity matrix was computed as listed in Table 4.

In Member 1 (i.e., the two outside contact bodies), the first mode's sensitivity was much higher than the eighth mode's sensitivity on the structural change (e.g., change in contact boundary condition). In Member 2 (i.e., the inside flexural beam), the sensitivity of the eighth mode was relatively higher than that of the first mode. Overall, modal sensitivities of Member 2 were much higher than those of Member 1. This indicates that any changes in structural parameters of Member 2 dominate the variation of dynamic characteristics of Interface 1.

Table 3 Damage scenarios to simulate natural frequency changes of Interface 1

| Mode | Natural Frequency (kHz) | | |
|---|---|---|---|
| | Intact | Damage 1 ($\alpha_1$=0.1; $\alpha_2$=0 ) | Damage 2 ($\alpha_1$=0; $\alpha_2$=0.1 ) |
| 1 | 20.365 | 20.095 | 19.67 |
| 8 | 81.524 | 81.355 | 78.091 |

Table 4 Modal sensitivity matrix of Interface 1

| Mode | Modal Sensitivity | |
|---|---|---|
| | Member 1 | Member 2 |
| 1 | 0.2819 | 0.7181 |
| 8 | 0.0478 | 0.9522 |

Table 5 Damage scenarios to simulate natural frequency changes of Interface 2

| Mode | Natural Frequency (kHz) | | |
|---|---|---|---|
| | Intact | Damage 1 ($\alpha_1$=0.1; $\alpha_2$=0 ) | Damage 2 ($\alpha_1$=0; $\alpha_2$=0.1 ) |
| 1 | 19.016 | 18.797 | 18.314 |
| 4 | 37.923 | 37.759 | 36.334 |

Table 6 Modal sensitivity matrix of Interface 2

| Mode | Modal Sensitivity | |
|---|---|---|
| | Member 1 | Member 2 |
| 1 | 0.2401 | 0.7599 |
| 4 | 0.0952 | 0.9048 |

#### *4.3.3 Modal sensitivity of interface 2*

Another FE model was established for the geometry and boundary conditions of Interface 2. The modal sensitivity matrix was estimated as follows: firstly, two damage scenarios were introduced into the FE model; secondly, two eigenvalues of mode 1 and mode 4 (shown in Fig. 14) were calculated as listed in Table 5; thirdly, the fractional changes of the two eigenvalues were computed and modal sensitivity matrix was computed as listed in Table 6.

In Member 1 (i.e., the two outside contact bodies), the sensitivity of the first mode was much higher than that of the fourth mode on the structural change (e.g., change in contact boundary condition). In Member 2 (i.e., the inside flexural beam), the fourth mode's sensitivity was relatively higher to the first mode's one. Generally, modal sensitivities of Member 2 were much higher than those of Member 1. It is noted that the change in structural parameters of Member 2 dominates the variation of dynamic characteristics of Interface 2. It is also noted that the modal sensitivities of Interface 2 are relatively stable than those of Interface 1.

## 5. Conclusions

In this study, local dynamic characteristics of mountable PZT interfaces were numerically analyzed to verify their feasibility on impedance monitoring of the prestress-loss in tendon anchorage subsystems. Firstly, a prestressed tendon-anchorage system with mountable PZT interfaces was described. Two types of mountable interfaces (which are different in geometric and boundary conditions) were designed for impedance monitoring in the tendon-anchorage subsystems. Secondly, laboratory experiments were performed to evaluate the impedance monitoring via the two mountable PZT interfaces placed on the tendon-anchorage under the variation of prestress forces. Impedance features such as frequency-shifts and root-mean-square-deviations were quantified for the two PZT interfaces. Finally, local dynamic characteristics of the two PZT interfaces were numerically analyzed to verify their performances on impedance monitoring at the tendon-anchorage system. For the two PZT interfaces, the relationships between structural parameters and local vibration responses were examined by modal sensitivity analyses.

From the experimental tests on the two interfaces, at least three major results were observed as follows: firstly, the impedance responses measured via the two interfaces had two dominant peaks which were sensitive to the change of prestress forces; secondly, the sensitive frequency ranges were shifted as the geometry and boundary condition of the interface were changed; and finally,

the PZT interface with the larger bonding area revealed much higher sensitivity for the indication of the prestress-loss.

From the analyses of dynamic characteristics of the mountable interfaces, at least four main results were observed as follows: firstly, there existed vibration modal shapes (longitudinal flexural and lateral flexural motions) which were matching to piezoelectric responses (longitudinal and lateral deformations) of the PZT patch on the interface; secondly, the second modal frequencies of the two interfaces matching to the second impedance peaks of them were reduced as the interface's widths were increased; thirdly, the change in structural parameters of the inner flexural section of the interface dominated the variation of dynamic characteristics which were corresponding to the change in impedance responses of the interface; and finally, the modal sensitivities of the PZT interface with the larger bonding area were relatively stable. As for the future work, the effect of the mother structure (e.g., tendon-anchorage subsystem) on the local resonance frequencies of the PZT interface should be investigated by the dynamic analysis.

## Acknowledgments

This research was supported by a grant (code 12 Technology Innovation E09) from Construction Technology Innovation Program funded by Ministry of Land, Transportation and Maritime Affairs (MLTM) of Korean government. The graduate students involved in this research were also partially supported by the Brain Korea 21 Plus program of Korean Government.

## References

Bhalla, S. and Soh, C.K. (2003), "Structural impedance based damage diagnosis by piezo-transducers", *Earthq. Eng. Struct. D.*, **32**(12), 1897-1916.

COMSOL, Inc. (2013), http://www.comsol.com

Efunda, Inc. (2010), http://www.efunda.com

Ho, D.D, Ngo, T.M. and Kim, J.T. (2014), "Impedance-based damage monitoring of steel column connection: numerical simulation", *Struct. Monit. Maint.*, **1**(3), 339-356.

Huynh, T.C. and Kim, J.T. (2014), "Impedance-based cable force monitoring in tendon-anchorage using portable PZT-interface technique", *Math. Probl. Eng.*, **2014**, Article ID 784731, 11 pages.

Huynh, T.C., Park, Y.H., Park, J.H. and Kim, J.T. (2014), "Feasibility verification of mountable PZT-interface for impedance monitoring in tendon-anchorage", *Shock Vib*., **2014**, Article ID 262975, 11 pages.

Kim, J.T., Park, J.H., Hong, D.S., Cho, H.M., Na, W.B. and Yi, J.H. (2009), "Vibration and impedance monitoring for prestress-loss prediction in PSC girder bridges", *Smart Struct. Syst.*, **5**(1), 81-94.

Kim, J.T., Huynh, T.C. and Lee, S.Y. (2014), "Wireless structural health monitoring of stay cables under two consecutive typhoons", *Struct. Monit. Maint.*, **1**(1), 47-67.

Kim, J.T., Nguyen, K.D. and Park, J.H. (2012), "Wireless impedance sensor node and interface washer for damage monitoring in structural connections", *Adv. Struct. Eng.*, **15**(6), 871-885.

Kim, J.T., Na, W.B., Park, J.H. and Hong, D.S. (2006), "Hybrid health monitoring of structural joints using modal parameters and EMI signatures", *Proceeding of SPIE,* San Diego, USA.

Kim, J.T., Park, J.H., Hong, D.S. and Park, W.S. (2010), "Hybrid health monitoring of prestressed concrete girder bridges by sequential vibration-impedance approaches", *Eng. Struct.*, **32**, 115-128.

Kim, J.T. and Stubbs, N. (1995). "Model-uncertainty impact and damage-detection accuracy in plate girder", *J. Struct. Eng. - ASCE*, **121**(10), 1409-1417.

Li, H.N, Yi, T.H., Ren L., Li, D.S. and Huo, L.S. (2014), "Review on innovations and applications in structural health monitoring for infrastructures", *Struct. Monit. Maint.*, **1**(1), 1-45.

Liang, C., Sun, F.P. and Rogers, C.A. (1994), "Coupled electro-mechanical analysis of adaptive material - Determination of the actuator power consumption and system energy transfer", *J. Intel. Mat. Syst. Str.*, **5**, 12-20.

Liang, C., Sun, F.P. and Rogers, C.A. (1996), "Electro-mechanical impedance modeling of active material systems", *Smart Mater. Struct.*, **5**(2), 171-186.

Lynch, J.P., Wang, W., Loh, K.J., Yi, J.H. and Yun, C.B. (2006), "Performance monitoring of the Geumdang Bridge using a dense network of high-resolution wireless sensors", *Smart Mater. Struct.*, **15**(6), 1561-1575.

Mascarenas, D.L., Todd, M.D., Park, G. and Farrar, C.R. (2007), "Development of an impedance-based wireless sensor node for structural health monitoring", *Smart Mater. Struct.*, **16**(6), 2137-2145.

Nguyen, K.D. and Kim, J.T. (2012), "Smart PZT-interface for wireless impedance-based prestress-loss monitoring in tendon-anchorage connection", *Smart Struct. Syst.*, **9**(6), 489-504.

Park, J.H., Kim, J.T., Hong, D.S., Mascarenas, D. and Lynch, J.P. (2010), "Autonomous smart sensor nodes for global and local damage detection of prestressed concrete bridges based on accelerations and impedance measurements", *Smart Struct. Syst.*, **6**(5), 711-730.

Park, G., Cudney, H.H. and Inman, D.J. (2001), "Feasibility of using impedance-based damage assessment for pipeline structures", *Earthq. Eng. Struct. D.*, **30**(10), 1463-1474.

Park, G.., Sohn, H., Farrar, C. and Inman, D. (2003), "Overview of piezoelectric impedance-based health monitoring and path forward", *Shock Vib. Digest*, **35**(6), 451-463.

Providakis, C., Stefanaki, K., Voutetaki, M., Tsompanakis, J. and Stavroulaki, M. (2014), "A near and far-field monitoring technique for damage detection in concrete structures", *Struct. Monit. Maint.*, **1**(2), 159-171.

Rice, J.A., Mechitov, K., Sim, S.H., Nagayama, T., Jang, S., Kim, R., Spencer, Jr, B.F., Agha, G. and Fujino, Y. (2010), "Flexible smart sensor framework for autonomous structural health monitoring", *Smart Struct, Syst.*, **6**(5-6), 423-438.

Sun, F.P., Chaudhry Z., Liang, C. and Rogers C.A. (1995), "Truss structure integrity identification using PZT sensor-actuator", *J. Intel. Mat. Syst. Str.*, **6**(1),134-139.

Yang, Y., Hu, Y. and Lu, Y. (2008), "Sensitivity of PZT impedance sensors for damage detection of concrete structures", *Sensors*, **8**(1), 327-346.

Zagrai, A. N. and Giurgiutiu, V. (2001), "Electro-mechanical impedance method for crack detection in thin plates", *J. Intel. Mat. Syst. Str.*, **12**(10), 709-718.